Inorganic Chemistry

Article

pubs.acs.org/IC

Single-Source-Precursor Synthesis of Hafnium-Containing Ultrahigh-Temperature Ceramic Nanocomposites (UHTC-NCs)

Jia Yuan,[†] Stefania Hapis,[‡] Hergen Breitzke,[§] Yeping Xu,[§] Claudia Fasel,[†] Hans-Joachim Kleebe,[‡] Gerd Buntkowsky,[§] Ralf Riedel,[†] and Emanuel Ionescu*[,†]

[†]Technische Universität Darmstadt, Institut für Materialwissenschaft, Jovanka-Bontschits-Strasse 2, D-64287, Darmstadt, Germany

[‡]Technische Universität Darmstadt, Institut für Angewandte Geowissenschaften, Schnittspahnstrasse 9, D-64287 Darmstadt, Germany

[§]Technische Universität Darmstadt, Eduard-Zintl-Institut für Anorganische und Physikalische Chemie, Alarich-Weiss-Strasse 4, D-64287 Darmstadt, Germany

ABSTRACT: Amorphous SiHfBCN ceramics were prepared from a commercial polysilazane (HTT 1800, AZ-EM), which was modified upon reactions with $Hf(NEt_2)_4$ and $BH_3{\cdot}SMe_2$, and subsequently cross-linked and pyrolyzed. The prepared materials were investigated with respect to their chemical and phase composition, by means of spectroscopy techniques (Fourier transform infrared (FTIR), Raman, magic-angle spinning nuclear magnetic resonance (MAS NMR)), as well as X-ray diffraction (XRD) and transmission electron microscopy (TEM). Annealing experiments of the SiHfBCN samples in an inert gas atmosphere (Ar, N_2) at temperatures in the range of 1300−1700 °C showed the conversion of the amorphous materials into nanostructured UHTC-NCs. Depending on the annealing atmosphere, HfC/HfB_2/SiC (annealing in argon) and HfN/Si_3N_4/SiBCN (annealing in nitrogen) nanocomposites were obtained. The results emphasize that the conversion of the single-phase SiHfBCN into UHTC-NCs is thermodynamically controlled, thus allowing for a knowledge-based preparative path toward nanostructured ultrahigh-temperature stable materials with adjusted compositions.

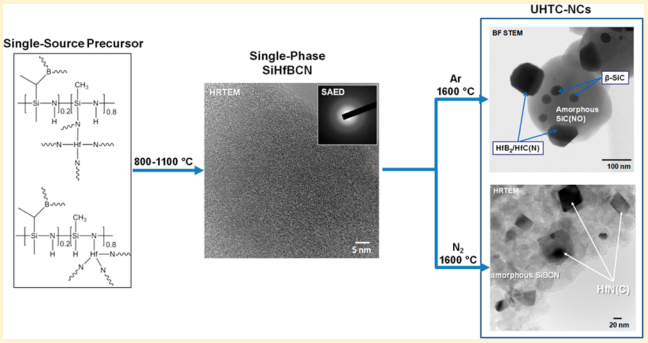

I. INTRODUCTION

When operated at (ultra)high temperatures and in extreme environments, structural parts and components are exposed to additional and more-severe design constraints, compared to those used in service at or near ambient temperature.[1−3] A fundamental property that is required in order to be able to operate materials at (ultra)high temperatures is related to their melting point. Naturally, (ultra)high melting points of the chosen materials are necessary, since, usually, the maximum operation temperature of a material is, with some exceptions, approximately half of its melting point.

Generally, high tolerance to thermal and mechanical stress is desirable in order to avoid catastrophic failure of the materials during operation. Thus, a high compliance to thermal stress can be provided by using highly thermoshock resistant materials. In addition, suitable, optimized ductility of the materials or, in the case of brittle components, such as ceramic-based materials, improved fracture toughness is desirable in order to provide high tolerance to mechanical stresses. Finally, no phase transformation of the materials in the range from the ambient to the operation temperature may occur, since those processes usually are accompanied by significant volume changes, which consequently might generate tremendous stresses and induce a catastrophic failure of the component. In the case of amorphous materials, an increased crystallization resistance may be beneficial for avoiding the generation of mechanical stress upon operation at (ultra)high temperatures.

Intense efforts have been made in the last decades in order to accommodate those requirements, which are often strongly conflicting. Thus, several types and classes of (ultra)high-temperature materials have been proposed and developed over the years, such as highly refractory metals, intermetallics/alloys, metal matrix composites (MMCs) as well as UHTCs or ceramic matrix composites (CMCs).

One effective preparative method to provide materials solutions for applications at (ultra)high temperatures and under extreme environments consists of the combination of UHTC materials (such as Group IV transition-metal diborides, carbides, or nitrides, being responsible for providing ultra-refractoriness[1,4,5]) with a silica former component (silicon-containing materials such as SiC, Si_3N_4, TaSi, $MoSi_2$ etc. being capable to generate a layer of dense silica-based scale at the surface upon exposure to aggressive environments). Especially ZrB_2/SiC and HfB_2/SiC (with ca. 20 vol % SiC) composites

Received: June 25, 2014
Published: September 18, 2014

have been reported to exhibit promising environmental behavior at (ultra)high temperatures.[6−8]

Single-source-precursor synthesis approaches have been used in recently to generate nanoscaled ceramic composites, some of them showing excellent behavior at ultrahigh temperatures and even in harsh environments.[9−15] The preparation of nanocomposite materials from single-source precursors represents a highly promising approach toward tailor-made phase compositions, morphologies, and microstructures and, consequently, specific property profiles.[16,17] Thus, Si_3N_4−TiN ceramics consisting of TiN nanoparticle homogeneously dispersed within a Si_3N_4-based matrix were prepared starting from a single-source precursor, which was synthesized upon reaction of perhydropolysilazane (PHPS) with $Ti(N(CH_3)_2)_4$.[18] Also carbidic and boride-based UHTCs were prepared from suitable single-source precursors, such as ZrC/SiC[19] and ZrC/ZrB_2[20] nanocomposites, which were obtained upon chemical modification of $Cp_2Zr(CH{=}CH_2)_2$ (Cp = cyclopentadienyl) with polymethylsilane and borane, respectively.[21] However, there is only scarce information in the literature concerning the single-source-precursor synthesis of UHTC-NCs.

In the present work, novel Hf-based ceramic nanocomposites were successfully prepared from a suitable single-source precursor and their behavior (i.e., thermal stability concerning decomposition, crystallization behavior) at temperatures up to 1800 °C was assessed and shown to be thermodynamically controlled. The presented results emphasize a convenient preparative approach to nanostructured ultrahigh-temperature stable materials (UHTC-NCs) starting from a greatly flexible/compliant single-source precursor.

II. EXPERIMENTAL PROCEDURE

1. Materials Synthesis. The synthesis of the polymeric single-source precursors was carried out in a purified argon atmosphere using the Schlenk technique. A quantity of 10.8 mL of Polysilazane HTT 1800 (Clariant, Sulzbach am Taunus, Germany) was dissolved in anhydrous toluene in a 250-mL three-necked Schlenk flask equipped with inlet connection and magnetic stirrer. Then, 1.2 or 4.8 mL (10 vol % and 30 vol %, with respect to HTT1800) of tetrakis(diethylamido)hafnium ($Hf(N(Et)_2)_4$, Sigma−Aldrich), was dissolved in 20 mL of toluene and added dropwise to the solution of HTT 1800 at ambient temperature. The mixture was stirred for 2 h at room temperature, then cooled to −50 °C by using isopropanol and dry ice. A volume of 2.4 or 0.6 mL of borane dimethyl sulfide complex ($BH_3{\cdot}(CH_3)_2S$, Sigma−Aldrich) was dissolved in 10 mL of toluene and added dropwise to the mixture solution, which was subsequently stirred for 2 h at −50 °C, then allowed to reach room temperature and stirred for 24 h. After the removal of the solvent in vacuum at 50−60 °C, a viscous liquid was obtained. The obtained single-source precursors were cross-linked at 200 °C (heating rate of 50 °C/h, dwelling time of 3 h) to produce yellow solids, which were warm-pressed at 260 °C and 63 MPa (P/O Weber, Remshalden, Germany, mold diameter = 10 mm). The obtained green bodies were pyrolyzed at 1100 °C (heating rate = 50 °C/h, dwell time = 2 h) to obtain the SiHfBCN ceramic monoliths. In order to investigate the high-temperature behavior of SiHfBCN, the amorphous ceramic samples were annealed in a high-temperature graphite furnace at 1300, 1500, and 1700 °C in argon or nitrogen atmosphere. In the subsequent discussion a nomenclature code for the prepared SiHfBCN ceramics will be used as described in Table 1.

2. Materials Characterization. The synthesized single-source precursors were analyzed by means of attenuated total reflection−Fourier transform infrared spectroscopy (ATR-FTIR) on a Bruker Vertex 70 FT-IR instrument (Bruker, USA). Thermogravimetry coupled with evolved gas analysis (EGA, i.e., *in situ* mass spectrometry, QMS 403C Aëolos, IPI and FTIR Tensor 27, Bruker Optics) was performed in argon atmosphere (Model STA 449C Jupiter, Netzsch Gerätebau GmbH).

Table 1. SiHfBCN-Based Samples Prepared within the Present Study

No.	sample name	HTT 1800:$Hf(NEt_2)_4$ volume ratio	annealing temperature (°C)	annealing atmosphere
1	SiHfBCN1a_1300	90:10	1300	Ar
	SiHfBCN1a_1500	90:10	1500	Ar
	SiHfBCN1a_1700	90:10	1700	Ar
2	SiHfBCN1b_1300	90:10	1300	N_2
	SiHfBCN1b_1500	90:10	1500	N_2
	SiHfBCN1b_1700	90:10	1700	N_2
3	SiHfBCN2a_1300	70:30	1300	Ar
	SiHfBCN2a_1500	70:30	1500	Ar
	SiHfBCN2a_1700	70:30	1700	Ar
4	SiHfBCN2b_1300	70:30	1300	N_2
	SiHfBCN2b_1500	70:30	1500	N_2
	SiHfBCN2b_1700	70:30	1700	N_2

All MAS NMR experiments were performed on a Bruker Avance II+ spectrometer at 400 MHz proton resonance frequency, employing a Bruker 4-mm double resonance MAS probe at spinning rates of 12 kHz at room temperature. Single-pulse (SP) ^{29}Si NMR spectra were recorded using a 90° pulse of 9 μs and recycle delays of 120 s. In contrast to SP ^{13}C NMR spectra, a 90° pulse of 4 μs and recycle delays of 20 s were adopted. ^{29}Si and ^{13}C NMR chemical shifts were externally referenced to tetramethylsilane ($Si(CH_3)_4$, TMS). In the case of ^{11}B NMR, chemical shifts were referenced, with respect to trimethyl borate.

For elemental analysis, a carbon analyzer Leco C-200 (Leco Corporation, USA) was used to determine the carbon content and a Model Leco TC-436 N/O analyzer (Leco Corporation, USA) to determine the oxygen content in the samples. The hafnium content was estimated from energy-dispersive X-ray spectroscopy (EDS) which was performed with an EDAX Genesis spectrometer (FEI, Eindhoven, The Netherlands) attached to a high-resolution scanning electron microscopy (HR-SEM) system (Philips, Eindhoven, The Netherlands). The samples were sputtered with a gold layer prior to investigation.

Powder X-ray diffraction (XRD) was obtained in flat-sample transmission geometry on a STOE Model STAD1 P system equipped with monochromatic Mo Kα radiation.

Transmission electron microscopy (TEM) measurements were performed using a Model JEM2100F (JEOL, Tokyo, Japan) operating at 200 kV. The samples were pulverized and dropped on a carbon-coated copper grid, followed by a light carbon coating to minimize charging under the incident electron beam.

III. RESULTS AND DISCUSSION

1. Synthesis of the Single-Source Precursors. Novel hafnium-containing polymeric single-source precursors for the synthesis of SiHfBCN ceramics were successfully prepared starting from a commercially available polysilazane containing Si−H and Si-vinyl groups (HTT 1800). The polymer was chemically modified in a first step upon reaction with tetrakis(diethylamido)hafnium complex. In a second step, the hafnium-containing polymer was reacted with borane-dimethyl sulfide complex and led to the single-source precursor for the SiHfBCN ceramics.

The chemical modification of the polysilazane HTT 1800 with $Hf(NEt_2)_4$ and $BH_3{\cdot}SMe_2$ was investigated by FTIR spectroscopy. In Figure 1a, FTIR spectra of the pure

dx.doi.org/10.1021/ic501512p | Inorg. Chem. 2014, 53, 10443−10455

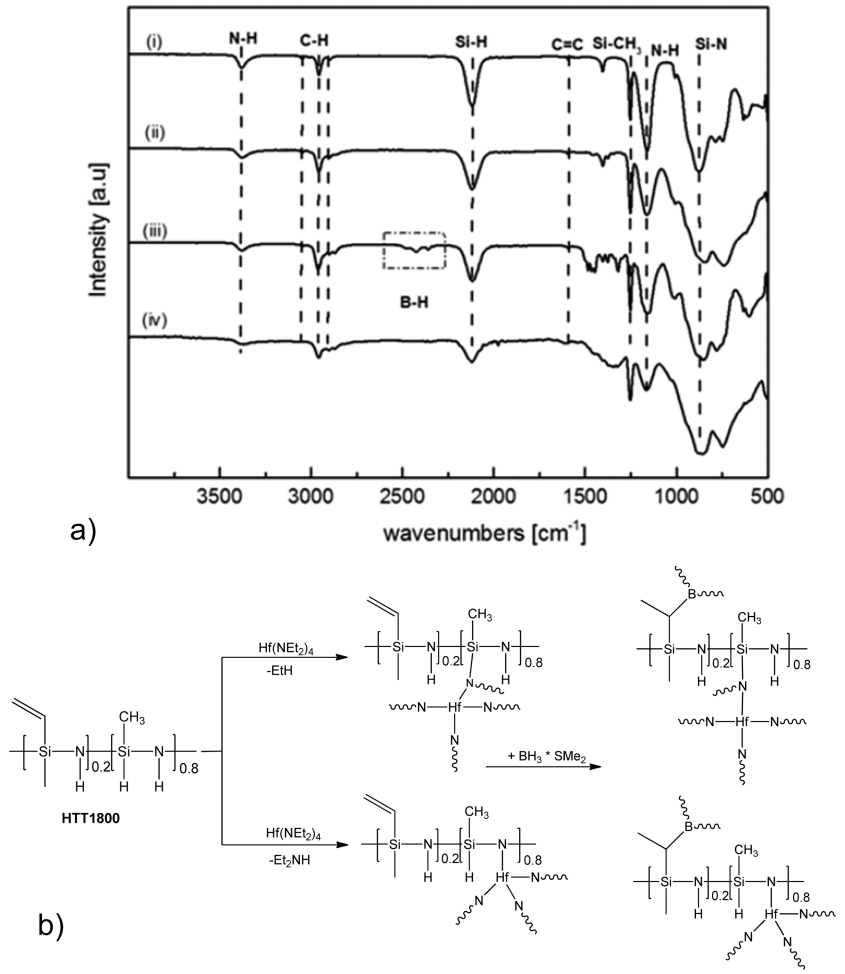

Figure 1. (a) FTIR spectra of HTT1800 (spectrum i), $Hf(NEt_2)_4$-modified HTT1800 (spectrum ii), and HTT1800 modified with $Hf(NEt_2)_4/BH_3{\cdot}SMe_2$ (spectrum iii), as well as HTT 1800 modified with $Hf(NEt_2)_4/BH_3{\cdot}SMe_2$ and cross-linked at 200 °C (spectrum iv). (b) Proposed reaction pathway of HTT 1800 with $Hf(NEt_2)_4$ and $BH_3{\cdot}SMe_2$.

polysilazane, as well as after reaction with $Hf(NEt_2)_4$ and subsequent modification with $BH_3{\cdot}SMe_2$, are shown. In the FTIR spectrum of HTT 1800, typical absorption bands related to C−H (2960 and 2965 cm^{-1}), N−H (3378 cm^{-1}), Si−H (2124 cm^{-1}), Si−N−H (1160 cm^{-1}), and Si−N (930 cm^{-1}) groups were observed.

The chemical modification of HTT 1800 with $Hf(NEt_2)_4$ induces a decrease in the intensity of the absorption bands related to N−H and Si−H groups, indicating that the reaction occurs at the Si−H/N−H substituents of HTT 1800 (see Figure 1b); whereas the vinyl groups in HTT 1800 (absorption bands at 3053 and 1598 cm^{-1}) were shown to not be affected by the reaction with the hafnium amido complex. A similar chemical reactivity of HTT 1800, i.e., reaction at both Si−H and N−H groups of the polymers, was also shown in the case of the reaction of HTT 1800 with a hafnium alkoxide.[10] Upon the addition of $BH_3{\cdot}SMe_2$, a hydroboration of the vinyl groups of HTT 1800 occurs (Figure 1b). However, the presence of absorption bands related to the vinyl groups (3053 cm^{-1}(=C−H), 1598 cm^{-1}(C=C)), as well as to B−H bonds (2477 cm^{-1}), in the Hf- and B-containing single-source precursor illustrates that not all vinyl groups of the polysilazane are involved in the reaction; this might be related to steric hindrance effects upon chemical modification of the polysilazane.[22]

The FTIR spectrum of the polymer precursor cross-linked at 200 °C (Figure 1a) show the disappearance of the B−H bands and thus indicating that the occurrence of cross-linking reactions relies on hydroboration and dehydrocoupling within the polymeric backbone.

The ^{29}Si MAS NMR spectrum of the cross-linked polymer cured at 200 °C (Figure 2) exhibits a signal at −24 ppm, assigned to $SiHC^{(sp3)}N_2$ sites (compare to −35 ppm for $SiHC^{(sp2)}N_2$; see ref 23); furthermore, a signal at −31 ppm corresponds to $SiC^{(sp3)}N_3$ sites and a third signal at −3.5 ppm was attributed to $SiC^{(sp3)}{}_2N_2$ sites[23] (see Table 2). Thus, the ^{29}Si NMR data of the cross-linked single-source precursor indicate that the hydroboration and vinyl polymerization reactions occurring under those conditions led to the transformation of the sp^2 hybridized carbons of the vinyl groups into sp^3 carbon sites.[23] Moreover, all three signals show a low-field shift, as compared to other SiCN-based materials,[23] which might rely on the fact that Hf is bonded to SiC_xN_{4-x} tetrahedra and, thus, the electron density at the Si sites is decreased (see also the discussion below on the NMR data of the obtained ceramic nanocomposites). This indicates consequently that the chemical modification of HTT 1800 leads to the formation of a single-source precursor for SiHfBCN.

2. Polymer-to-Ceramic Conversion. The thermal conversion of the Hf- and B-containing single-source precursor

dx.doi.org/10.1021/ic501512p | Inorg. Chem. 2014, 53, 10443−10455

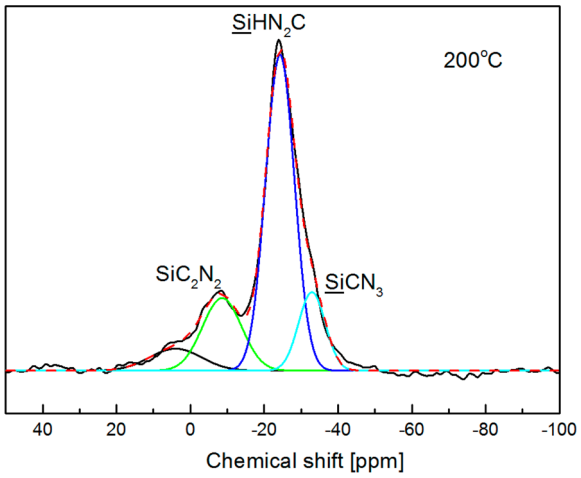

Figure 2. ^{29}Si MAS NMR spectrum of HTT 1800 modified with $Hf(NEt_2)_4$ and $BH_3{\cdot}SMe_2$ and cross-linked at 200 °C.

Table 2. Chemical Shifts and Site Fractions of SiC_2N_2, $SiHCN_2$, and $SiCN_3$ Sites Derived from Gaussian Line Fitting of the ^{29}Si NMR Spectrum in Figure 2

	SiC_2N_2		$SiHCN_2$		$SiCN_3$	
curing temperature (°C)	δ (ppm)	site fraction (%)	δ (ppm)	site fraction (%)	δ (ppm)	site fraction (%)
200	−3.5	26.2	−24	60.0	−31	13.8

into amorphous SiHfBCN was investigated by thermogravimetry (TGA) coupled with evolved gas analysis (EGA). Figure 3a indicates that the polymer-to-ceramic conversion occurs in three main steps (as can be seen from the DTG curve) and shows a ceramic yield of ca. 80 wt %. This is significantly higher than the ceramic yield of HTT 1800 (ca. 65 wt %) and is considered being a consequence of the strong increase of the cross-linking degree of the polymer upon modification with $Hf(NEt_2)_4$ and $BH_3{\cdot}SMe_2$. At temperatures beyond 800 °C, no mass loss was recorded, thus the polymer-to-ceramic transformation is considered to be completed up to this temperature. Cross-linking of the hafnium-containing polymeric precursor mainly relies on hydrosilylation and vinyl polymerization processes, as reported also for other Si−H and Si-vinyl substituted polysilazane-based polymers.[24−27] These processes occur without mass loss and contribute to the significant increase of the ceramic yield of the single-source precursor, as compared to the Hf- and B-free polysilazane. In addition, transamination processes between ≡Si−N═/≡Si−N and ≡Si−N═/≡Hf−N═ groups occur with the release of amine fragments, as indicated by mass spectrometry data during EGA (see Figure 3d). Thus, during the decomposition step at temperatures beyond 400 °C (Figures 3b−d), the mass loss relates to the evolution of hydrogen and methane, as well as ethane and diethylamino fragments. The hydrogen release is attributed to dehydrocoupling reactions occurring between Si−H and N−H or B−H and N−H groups, which lead to the formation of ≡Si−N═ and ═B−N═ linkage, respectively.[22,27] The release of methane and ethane occurs due to the decomposition of the organic substituents of the single-

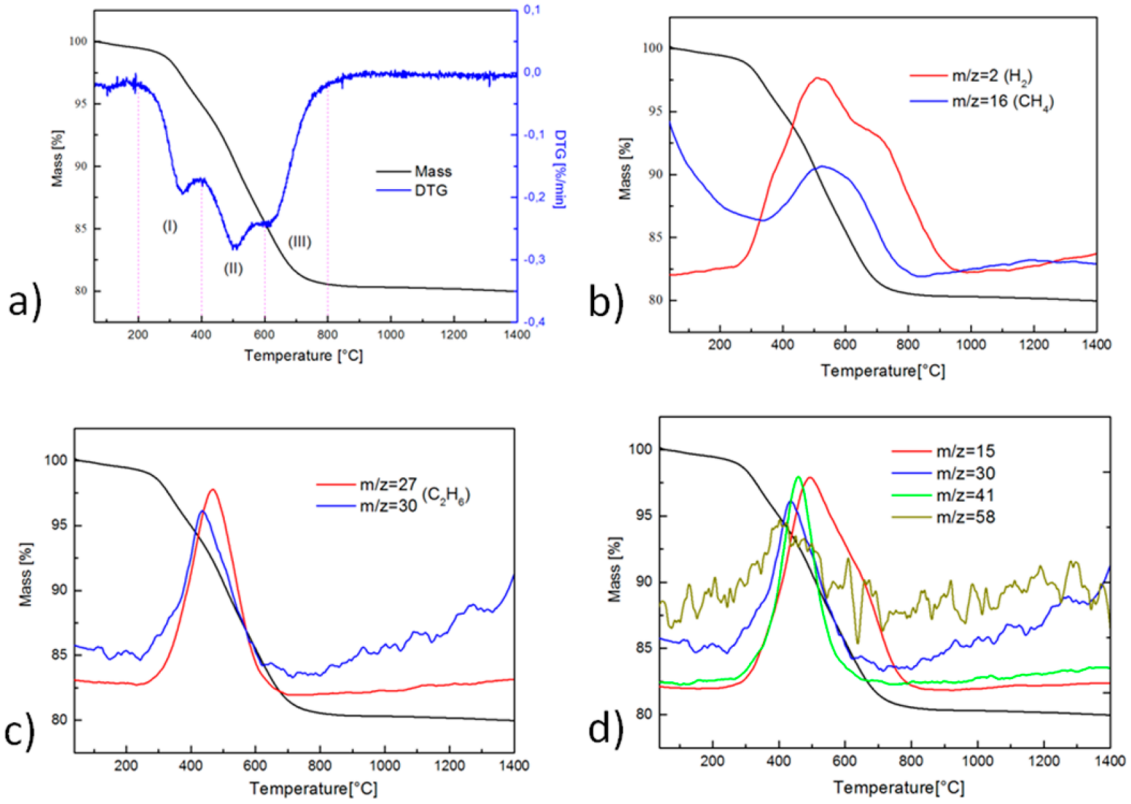

Figure 3. (a) Thermogravimetric analysis and (b−d) mass spectrometry quasi-multiple ion detection (QMID) ion current curves of cross-linked polysilazane (HTT 1800) modified with 30 vol % $Hf(NEt_2)_4$ and $BH_3{\cdot}S(CH_3)_2$ showing the release of (b) hydrogen and methane, (c) ethane, and (d) diethylamino fragments during the polymer-to-ceramic transformation.

dx.doi.org/10.1021/ic501512p | Inorg. Chem. 2014, 53, 10443−10455

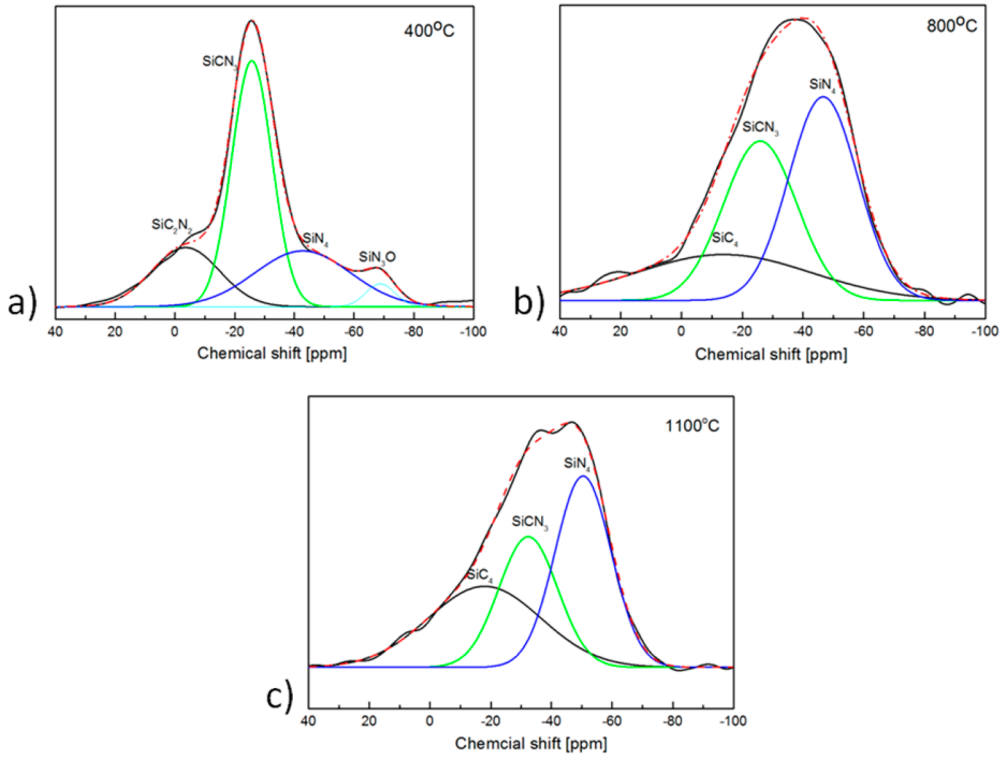

Figure 4. ^{29}Si MAS NMR spectra of the samples pyrolyzed at (a) 400, (b) 800, and (c) 1100 °C.

Table 3. Fraction of SiC_2N_2, SiC_4, and $SiCN_3$ and SiN_4 Sites Derived from Gaussian Line Fitting of the ^{29}Si NMR Spectra in Figure 4

	SiC_4		SiC_2N_2		$SiCN_3$		SiN_4	
curing temperature (°C)	δ (ppm)	site fraction (%)	δ (ppm)	site fraction (%)	δ (ppm)	site fraction (%)	δ (ppm)	site fraction (%)
400			−4	20.1	−26	49.8	−43	26.8
800	−14	23.8			−26	34.6	−47	41.6
1100	−18	33.2			−32	27.8	−48	39.0

source precursor; whereas the evolution of the diethylamino fragments is due to the decomposition of the $-NEt_2$ end groups in the precursor or on transamination processes between ≡Si–N═ and ≡Hf–N═ groups.

In addition to the TGA/EGA *in situ* investigation, *ex situ* MAS NMR spectroscopy was performed in order to attain more information about the polymer-to-ceramic process. Thus, ^{13}C, ^{29}Si, and ^{11}B MAS NMR spectra of samples obtained upon thermal treatment of the single-source precursor at 400, 800, and 1100 °C were measured.

The ^{29}Si MAS NMR spectra of the samples pyrolyzed between 400 °C and 1100 °C are shown in Figure 4.

The ^{29}Si NMR spectra (Figure 4) show signals for Si sites with bonds to C and N, i.e., SiC_xN_{4-x} ($0 \le x \le 4$) tetrahedra.[28] The chemical shift and the fractions of the different Si sites were evaluated upon deconvolution of the ^{29}Si NMR spectra and are summarized in Table 3. The ^{29}Si NMR spectrum of the sample pyrolyzed at 400 °C exhibit one peak at −26 ppm, which was attributed to $SiCN_3$ sites (site fraction = 49.8%). In addition, two signals at −4 and −43 ppm were attributed to $SiC_2(sp^3)N_2$ (20.1%) and SiN_4 (26.8%) sites, respectively. Upon increasing the pyrolysis temperature to 800 °C, the amount of $SiC_2(sp^3)N_2$ sites decreases as a result of transamination reactions and methane release, as also reported for a hafnium-alkoxide-modified polysilazane.[27] This is in good agreement with the EGA data, which indicate the evolution of methane and amino fragments in the same temperature range (see Figure 3). The ^{29}Si NMR spectra of the samples pyrolyzed at 800 and 1100 °C exhibit a new signal with a chemical shift at approximately −14 ppm, which has been assigned to SiC_4 sites and indicates demixing/partitioning processes occurring in the SiHfBCN samples, cf. SiC_xN_{4-x} = SiN_4 + SiC_4. This is somehow intriguing, because, at these temperatures, SiCN/SiBCN-based ceramics are typically assumed single-phasic and the intensity of the SiC_4 signal is usually very low. Interestingly, there is a high-field shift of the $SiCN_3$ and SiN_4 signals as the heat-treatment temperature increases. Thus, the signal of $SiCN_3$ sites shifts from −26 ppm (400 and 800 °C) to −32 ppm (at 1100 °C), indicating the presence of Hf in the secondary coordination sphere of the Si sites at temperatures up to 800 °C.[29] As the pyrolysis temperature increases to 1100 °C, the signal shifts toward high field, indicating Hf being released from the secondary coordination sphere of the Si sites at the mentioned temperature. In the case of the SiN_4 signal, this effect was even stronger: the chemical shift of the signal was −43, −47, and −48 ppm upon pyrolysis at 400, 800, and 1100 °C, respectively. Thus, it seems that Hf is released first from the coordination sphere of the SiN_4 sites, as compared to the $SiCN_3$ sites. Thus, the NMR data indicate that, probably, phase separation processes start in SiHfBCN at temperatures as low

dx.doi.org/10.1021/ic501512p | *Inorg. Chem.* 2014, 53, 10443−10455

as 800 °C. Currently, it is assumed that the modification of the polysilazane with hafnium might be responsible for this behavior. This effect (*viz*, demixing of mixed-bond SiC_xN_{4-x} tetrahedra) was also reported for a hafnium-alkoxide-modified polysilazane.[27] However, whereas in the case of the reported SiHfCNO, the hafnium incorporation induces a partitioning process, cf. $SiC_xN_{4-x} = SiN_4 + C$[27] (as known from silicon carbodiimide-derived SiCN materials),[17] in the present case partitioning of SiC_xN_{4-x} tetrahedra generates amorphous SiC in addition to Si_3N_4.[30−33] This finding clearly emphasizes that the chemical composition and molecular architecture of the single-source precursor has a crucial effect on the phase composition of the resulting nanocomposite material.[10]

The ^{13}C MAS NMR spectrum of the sample prepared at 400 °C exhibits a signal at 2 ppm, which was assigned to $Si-CH_3$ groups (Figure 5).[9] This signal was not found in the samples prepared at 800 and 1100 °C; as the pyrolysis of the polymeric precursor at those temperatures induces a drastic release of the methyl groups,[9,34] (e.g., CH_4 evolution, as detected by EGA) and the segregation of carbon, leading to the appearance of new signals in the ^{13}C NMR spectra (Figure 5). Thus, the ^{13}C spectrum of the sample pyrolyzed at 1100 °C indicates the presence of sp^2 C network, which, however, is thought to contain large amounts of C−N/C−B bonds (as indicated by the shifting of the signal from usually ca. 130 ppm in sp^2-carbon to ca. 145 ppm). This has been already reported in the literature for polymer-derived SiBCN ceramics, which also contain a segregated sp^2 C phase with C−N and C−B bondings representing interfaces between the carbon phase and SiN_x- and BN_x-based domains, respectively.[35,36] In addition, the spectra of the samples pyrolyzed at 800 and 1100 °C exhibit a signal at 28 ppm, which was assigned to CSi_4 sites and thus supports the findings of the ^{29}Si NMR data revealing a strong phase separation of the samples (which was not observed in the case of ternary SiCN ceramics[37,38]); obviously, the simultaneous incorporation of Hf and B into the preceramic polysilazane fundamentally affects its ceramization behavior.

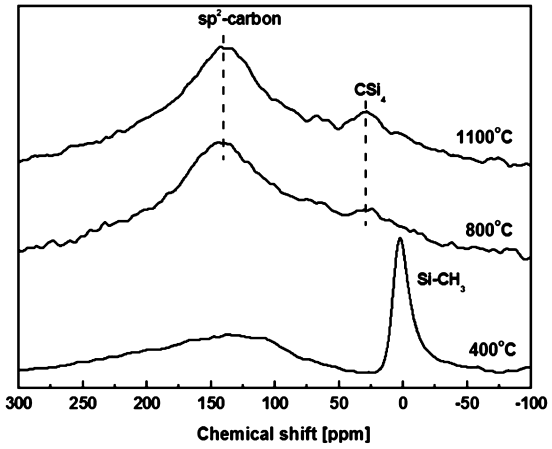

Figure 5. ^{13}C MAS NMR spectra of the SiHfBCN1 samples prepared upon pyrolysis of the single-source precursor at 400, 800, and 1100 °C.

The ^{11}B MAS NMR spectra of all prepared samples showed two main signals at 40 and 30 ppm, which were assigned to BCN_2 (major) and BN_3 (minor) sites, respectively (Figure 6).[36] Please note that, upon the hydroboration process of the hafnium-modified polysilazane, first, BC_3 sites are expected, which obviously undergo rearrangement reactions already at temperatures as low as 400 °C to convert into BCN_2 and BN_3. Considering the evolution of the Si sites with temperature (SiC_2N_2 sites get consumed and the amount of $SiCN_3$ decreases as the synthesis temperature increases; see Table 3 and Figure 4), we assume that the BC_3 units undergo exchange reactions with SiC_2N_2 sites to generate BCN_2 and SiC_4 units as follows: $BC_3 + SiC_2N_2 = BCN_2 + SiC_4$.[28] Similarly, the formation of BN_3 can be explained as $2BC_3 + 3SiC_2N_2 = 2BN_3 + 3SiC_4$ and $BC_3 + SiCN_3 = BN_3 + SiC_4$.

High-resolution transmission electron microscopy (HR-TEM) of the sample prepared at 1100 °C indicates an amorphous, featureless, and homogeneous microstructure (Figure 7). However, based on the MAS NMR data, the sample is highly nanoheterogeneous, thus having a complex phase composition, consisting of amorphous Si_3N_4, SiC, sp^2 C, HfN and BN phases showing mixed bonds at their interfaces (e.g., C−N/C−B bondings and BC_2N sites at the interface between C and BN).

3. High-Temperature Behavior. The SiHfBCN samples prepared upon pyrolysis at 1100 °C were annealed at 1300−1700 °C for 5 h in argon, as well as in a nitrogen atmosphere. In Figure 8, the mass loss upon annealing at different temperatures and atmospheres is shown. The samples did not exhibit any mass change after annealing at 1300 °C in an argon atmosphere, while annealing at 1500 °C in an argon atmosphere induced a mass loss of ca. 10 wt % in SiHfBCN1 (having low hafnium content) and ca. 6 wt % in SiHfBCN2 (ca.

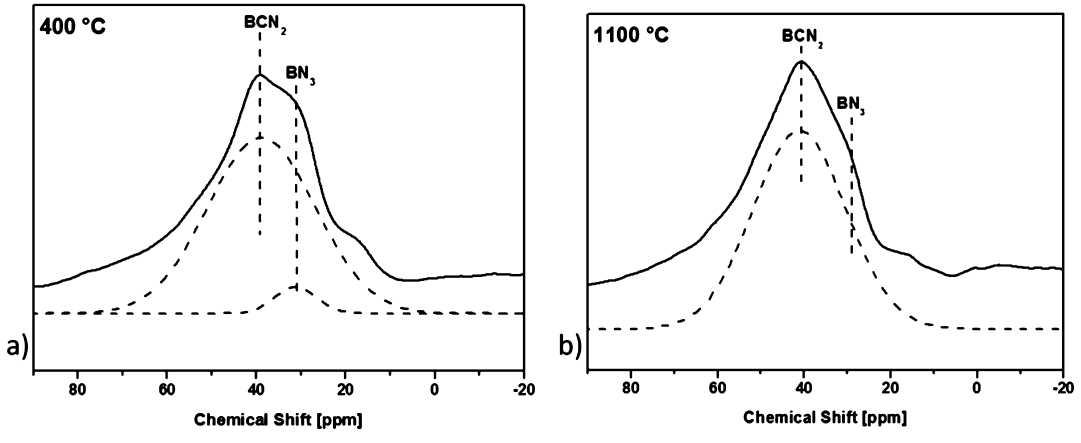

Figure 6. ^{11}B MAS NMR spectra recorded for the samples prepared at (a) 400 °C and (b) 1100 °C.

dx.doi.org/10.1021/ic501512p | *Inorg. Chem.* 2014, 53, 10443−10455

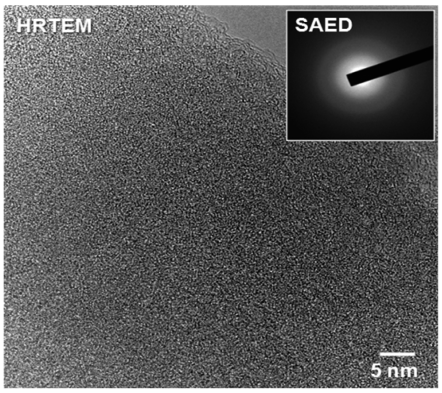

Figure 7. HR-TEM micrograph of a SiHfBCN2a powder sample prepared upon pyrolysis at 1100 °C indicating a homogeneous microstructure. The selected area electron diffraction (SAED, see inset) clearly shows the amorphous nature of the sample.

24 wt % Hf). Interestingly, the Hf- and B-free sample, SiCN, showed a significantly higher mass loss upon annealing under identical conditions, i.e., ca. 25 wt % (see Figure 8a).

The evolution of the SiCN ternary system can be described as consisting of three possible processes: (i) phase separation of the single-phase SiCN materials into a multiphasic material consisting of SiC_x and SiN_x nanodomains as well as excess C (no mass loss); (ii) carbothermal decomposition of the amorphous silicon nitride-rich regions, $SiN_x + C = \beta$-SiC + N_2 (accompanied by mass loss); (iii) decomposition of the amorphous silicon-nitride-rich regions into elements, $SiN_x = Si + N_2$ (mass loss). In our case, mainly processes (i) and (ii) contribute to the mass loss of SiCN upon annealing at high temperatures.[39] The significant improvement of the stability of SiCN concerning decomposition by means of Hf and B incorporation is obvious. There are numerous studies in the literature concerning the HT behavior of SiBCN ceramics. In the case of SiBCN, the improvement of the stability has been related to the presence of BC_xN_y phases which separate SiN_x-rich regions from excess carbon and thus kinetically inhibit the carbothermal decomposition of the materials. In addition, as the BC_xN_y phase is considered to encapsulate the SiN_x-rich regions, their decomposition into elements is also suppressed in SiBCN.[40]

In the case of our SiHfBCN samples, we similarly assume a kinetic stabilization of the materials upon Hf and B incorporation. The incorporation of Hf significantly increases the thermal stability of the ceramic system (SiHfCN samples show lower mass loss upon annealing at 1500 °C if compared to SiCN; data not shown here). This is thought to rely on the presence of HfN-rich regions, which are significantly more stable concerning their carbothermal decomposition than the SiN_x regions. Furthermore, boron is considered to have a similar effect as that in the previously mentioned SiBCN ceramics.[41] This is supported by our NMR findings, which indicate the presence of BCN_2 structural units which might be located at the interface between carbon and BN-rich regions (i.e., also, in our case, carbon and SiN_x regions are separated, and, thus, the carbothermal reaction is suppressed). The difference in the thermal stability of SiCN and SiHfBCN after annealing at 1700 °C in argon was even larger: thus, SiCN lost almost 50% of its mass upon annealing at 1700 °C for 5 h, whereas the SiHfBCN samples exhibited mass losses of ca. 30% (Figure 8).

The elemental analysis data shown in Table 4 clearly emphasize the effect of the carbothermal decomposition of SiN_x upon nitrogen release on the chemical composition of the samples (also note that, at 1700 °C, the decomposition of SiN_x into elements should be taken into account): the nitrogen content of SiHfBCN2a remains constant upon annealing at 1500 °C; whereas annealing of the sample at 1700 °C induces a strong depletion in nitrogen.

Annealing of the samples in a nitrogen atmosphere obviously showed, in all cases, significantly lower mass losses, compared to the annealing experiments performed in an argon atmosphere. Thus, the SiCN sample annealed at 1700 °C in nitrogen exhibited a mass loss of ca. 30%, whereas the SiHfBCN samples exhibited excellent behavior, with mass losses of <5 wt % (see Table 4). This finding clearly correlates with the nitrogen content of the samples, which does not significantly change after the HT annealing, indicating that both the carbothermal decomposition of SiN_x, as well its decomposition into elements are effectively suppressed.

The annealed SiHfBCN samples were investigated concerning phase composition and microstructure by X-ray diffraction and TEM. The as-prepared samples (pyrolysis at 1100 °C) were shown to be X-ray amorphous (Figures 9a and 9b). The

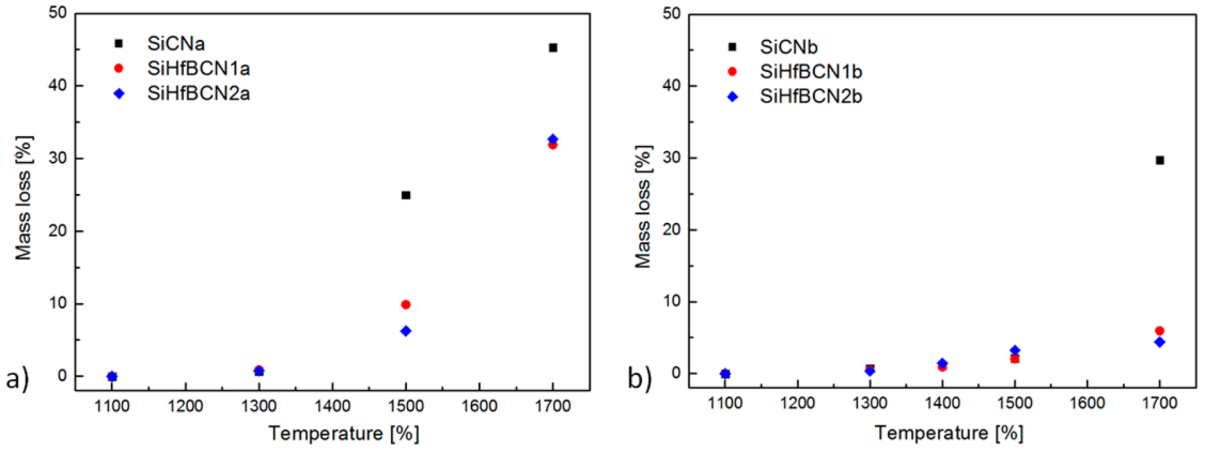

Figure 8. Mass loss of SiHfBCN and SiCN ceramics as a function of annealing temperature: (a) annealing experiments in an Ar atmosphere; (b) annealing in a N_2 atmosphere.

dx.doi.org/10.1021/ic501512p | Inorg. Chem. 2014, 53, 10443−10455

Table 4. Chemical Composition of SiHfBCN Samples after Annealing at Different Temperatures

sample	annealing temperature (°C)	mass loss (wt %)	shrinkage (vol %)	C (wt %)	O (wt %)	N (wt %)	Hf (wt %)[a]
SiHfBCN2a-1100	1100			12.7	2.4	18.4	22.5
SiHfBCN2a-1500	1500	6.3	10.7	16.4	1.7	19.1	25.2
SiHfBCN2a-1700	1700	35.0	27.2	20.7	0.9	0.4	28.6
SiHfBCN2b-1500	1500	3.1	8.5	11.4	2.4	23.8	27.3
SiHfBCN2b-1700	1700	4.4	14.5	12.3	1.6	20.7	23.3

[a]The hafnium content was estimated using EDS analysis.

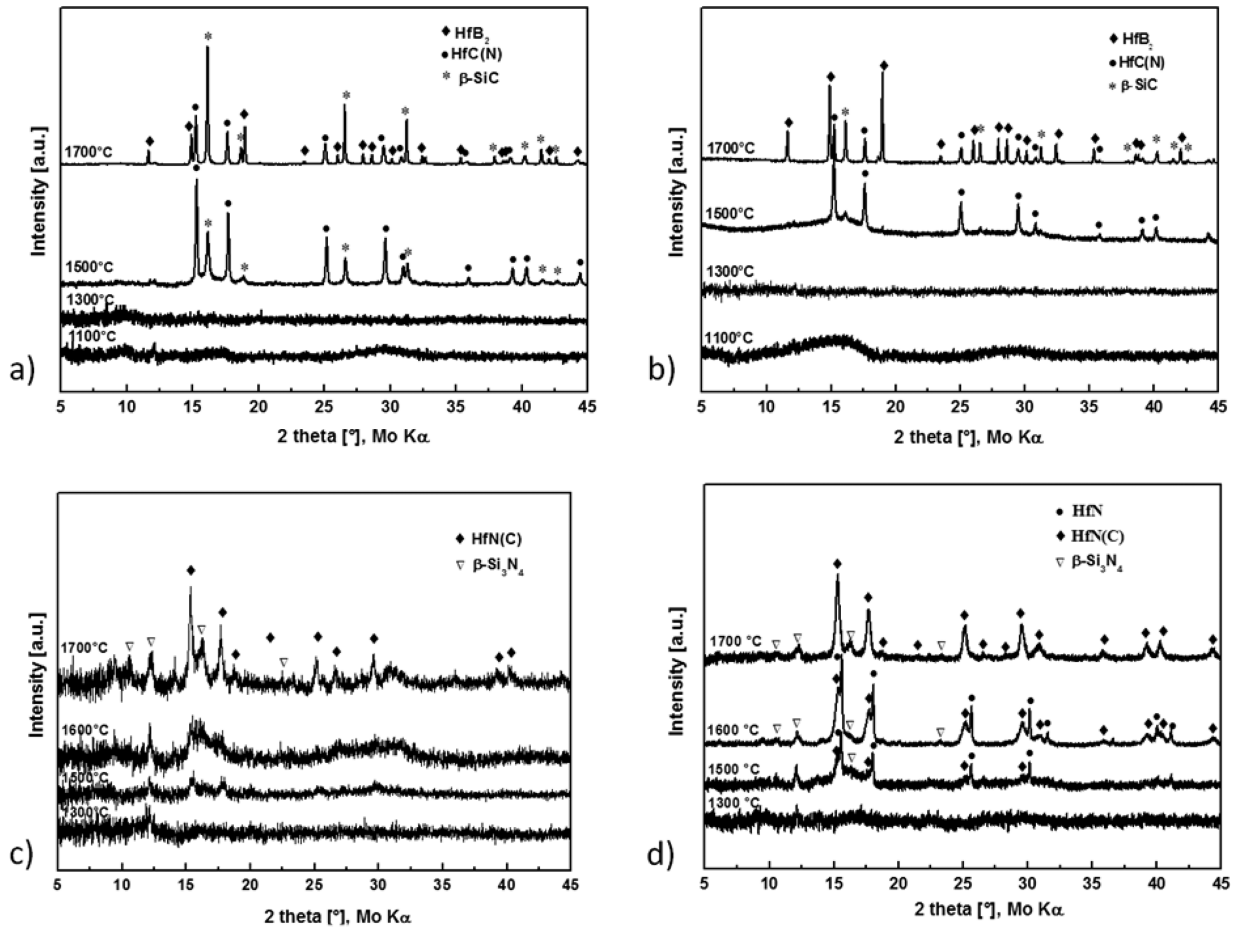

Figure 9. Crystallization behavior of SiHfBCN upon heat treatment at temperatures of 1300−1700 °C in Ar and N_2: (a) SiHfBCN1a and (b) SiHfBCN2a (argon atmosphere); (c) SiHfBCN1b and (d) SiHfBCN2b (nitrogen atmosphere).

samples do not crystallize upon annealing at 1300 °C in argon atmosphere, whereas after annealing at 1500 °C Hf(C_xN_{1-x}) and β-SiC crystallize. Upon annealing at 1700 °C, HfB_2 was identified as additional crystalline phase (see Figures 9a and 9b). The composition of Hf(C_xN_{1-x}) was estimated from the position of the reflections and upon using the Vegard's rule to be $HfC_{0.78}N_{0.22}$.

The crystallization processes occurring in SiHfBCN upon annealing at 1500−1700 °C in an argon atmosphere can be rationalized as follows:

(i) Based on the MAS NMR data, the as-prepared material is phase-separated and consists of SiN_x, SiC_x, excess carbon, BN, and HfN amorphous phases (although this description does not take into account mixed bondings at the interfaces between the different phases).

(ii) The amorphous SiN_x-rich regions can undergo a crystallization process to α-Si_3N_4 (detected in small amounts in the XRD patterns of the samples annealed at 1500 °C) as well as a carbothermal decomposition, cf. $SiN_x + C = \beta$-SiC + N_2, which induces the crystallization of silicon carbide. As previously mentioned, the incorporation of Hf and B suppresses the formation of β-SiC. This is clearly shown in the samples annealed at 1500 and 1700 °C, as the amount of β-SiC is reduced with increasing amount of Hf and B, as revealed by the Rietveld refinement of the X-ray diffraction patterns of the samples annealed in argon at 1700 °C (see Figure 10 and Table 5). Thus, the weight fraction of β-SiC (related to the crystalline content of the samples) decreases from 88% in SiHfBCN1a to 72% in SiHfBCN2a. Also, the crystallite size of β-SiC is shown to decrease from ca. 112 nm in SiHfBCN1a to ca. 50 nm in SiHfBCN2a (Table 5).

(iii) The presence of $HfC_{0.78}N_{0.22}$ (crystallite size of ca. 40 and 63 nm for SiHfBCN1a and SiHfBCN2a, respectively; see Table 5) can be explained as a result of the reaction of HfN with the excess carbon. In an subsequent step (annealing at 1700 °C), $HfC_{0.78}N_{0.22}$ reacts with the BN phase to generate

dx.doi.org/10.1021/ic501512p | Inorg. Chem. 2014, 53, 10443−10455

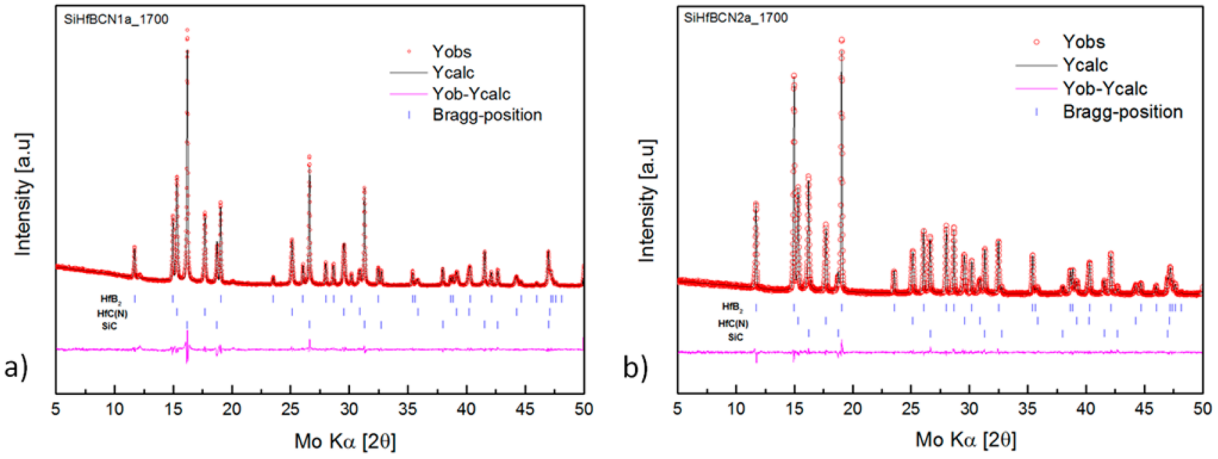

Figure 10. Result of Rietveld refinement of the SiHfBCN1 and SiHfBCN2 annealed in argon at 1700 °C. The positions of the Bragg reflections are indicated by vertical bars ("|"). The difference curve between the experimental and the calculated intensities from the refined model is shown in the lower part of the diagram.

Table 5. Weight Fractions (Relative to the Crystalline Content of the Investigated Samples) and Crystallite Size of HfB_2, HfC(N), and SiC for SiHfBCN1a and SiHfBCN2a Annealed at 1700 °C in Argon, as Determined from Rietveld Refinement of the XRD Data

	HfB_2		HfC(N)		SiC	
ceramic	fraction (wt %)	size (nm)	fraction (wt %)	size (nm)	fraction (wt %)	size (nm)
SiHfBCN1a	4.4	200.2	7.3	39.3	88.3	112.1
SiHfBCN2a	18.8	330.3	9.4	63.5	71.8	48.7

free carbon and HfB_2 (and probably some nitrogen is released), as it is known from the reactions of metal carbides with boron nitride.[42] The size of the HfB_2 precipitation is significantly larger than those of β-SiC and $HfC_{0.78}N_{0.22}$ (200 and 330 nm for SiHfBCN1a and SiHfBCN2a, respectively; see Table 5).

The information on the crystallization behavior of SiHfBCN obtained from the XRD data have been supported by TEM investigation. In Figure 11, the microstructure of SiHfBCN2a is shown, indicating the presence of an amorphous SiC(N,O)-based matrix and of β-SiC as well as HfC(N) and HfB_2 nanoprecipitations. The size of the β-SiC nanoparticles is ca. 30−50 nm; whereas the HfC(N) and HfB_2 precipitations were significantly larger (ca. 100−200 nm). Thus, the TEM results agree very well with the value obtained from the Rietveld refinement of the XRD data (Table 5).

The samples annealed in nitrogen atmosphere showed a significant effect of the Hf and B content on their crystallization behavior. Thus, the sample with low Hf and B content (SiHfBCN1) remains mainly X-ray amorphous, even up to 1600 °C; whereas SiHfBCN2 shows crystallization of β-Si_3N_4 and HfN upon annealing at 1500 °C. The crystalline HfN phase is shown to be consumed as the annealing temperature is increased to 1700 °C and instead a N-rich HfN_xC_{1-x} (i.e., $HfN_{0.52}C_{0.48}$) is generated (Figures 9c and 9d). This clearly supports the assumption that HfN-rich regions react with excess carbon to yield $HfN_{0.52}C_{0.48}$ (as it is also known from titanium carbonitrides[18]).

TEM micrographs of the sample SiHfBCN2b annealed at 1700 °C indicate the presence of the HfN_xC_{1-x} nanocrystallites with sizes of ca. 50 nm embedded within an amorphous SiBCN-based matrix (Figure 12). As it is known that HfN and SiBCN are materials that can withstand ultrahigh temperatures (i.e., beyond 2000 °C), the nanocomposite obtained upon nitrogen annealing of SiBCN2b is considered to be a UHTC-NC with promising behavior at ultrahigh temperatures and, because of the SiBCN matrix, even in harsh environments.

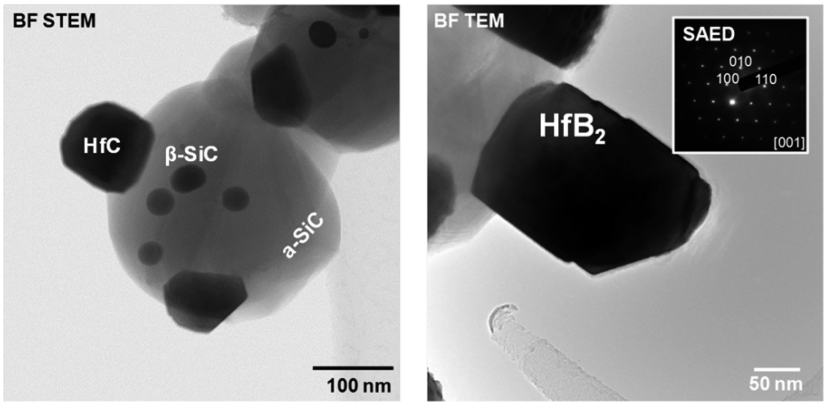

Figure 11. TEM micrographs of SiHfBCN2a annealed at 1700 °C in argon atmosphere. In the left micrograph HfC and β-SiC crystallites are shown; the matrix is SiC-based and amorphous; the micrograph on the right shows a HfB_2 crystallite, as identified by means of electron diffraction (see SAED shown as the inset).

dx.doi.org/10.1021/ic501512p | Inorg. Chem. 2014, 53, 10443−10455

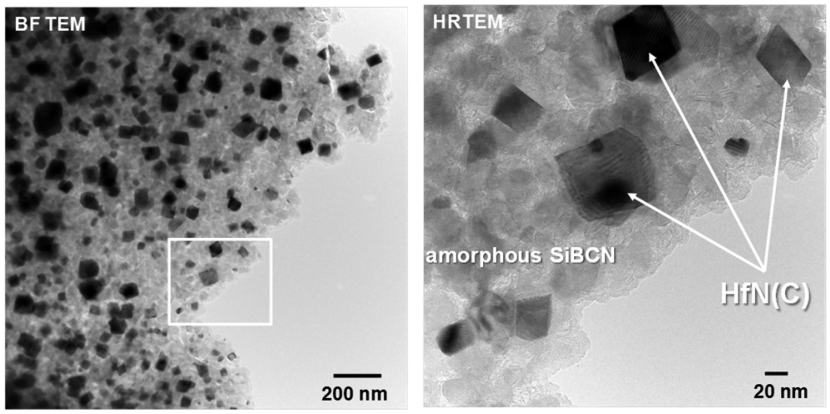

Figure 12. TEM micrographs of the sample SiHfBCN2b annealed at 1700 °C in nitrogen atmosphere showing HfN(C) nanoprecipitates embedded within an amorphous SiBCN matrix.

The ^{29}Si MAS NMR spectra of SiHfBCN2b annealed at 1300, 1500, and 1700 °C in a nitrogen atmosphere are shown in Figure 13. The chemical shift of the SiN_4 sites in the sample

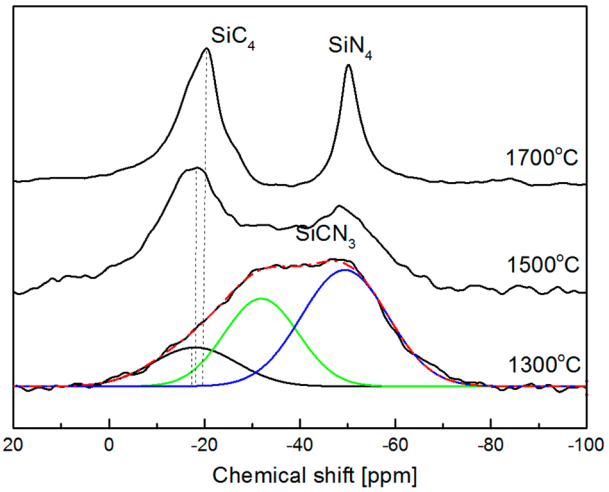

Figure 13. ^{29}Si MAS NMR spectra of SiHfBCN2b annealed in a nitrogen atmosphere at different temperatures.

annealed at 1300 °C was −49 ppm (Table 6), indicating that, at this temperature, HfN already phase separates (however, as an amorphous phase; see Figure 9d). Annealing of the sample at higher temperatures leads to a partitioning of the Si(B)CN phase; thus, the $SiCN_3$ sites (mixed-bond tetrahedra) disappear and instead SiC_4 and SiN_4 sites are present, showing the phase separation of the matrix into SiC and Si_3N_4 (Table 6), as also indicated by XRD and TEM results.

In order to rationalize the different processes occurring upon HT annealing of SiHfBCN in Ar and N_2 atmospheres, the change in the Gibbs free energy for some possible reactions was assessed (see the Ellingham diagram in Figure 14). The thermodynamic data presented in Figure 14 indicate that the

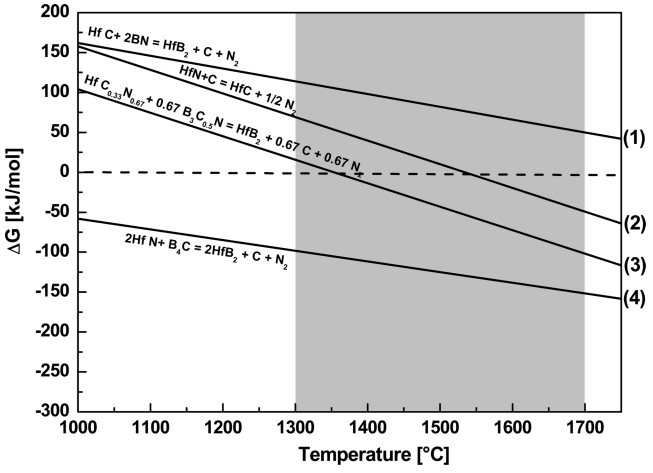

Figure 14. Temperature dependence of the change in the Gibbs free energy (Ellingham diagram) of different possible reactions occurring during HT annealing of SiHfBCN (data taken from ref 43). The ΔG value for reaction (3) in the figure has been estimated upon combining reactions (1) and (4) in the figure (cf. (3) = 0.67(1) + 0.33(4)). The gray shaded area indicates the temperature range of the high-temperature annealing experiments.

HfN phase, which is supposed to partition and crystallize from the single-phase SiHfBCN upon HT annealing, can react with segregated carbon to form HfC at temperatures beyond 1500 °C. This is indeed supported by the XRD data of the sample SiHfBCN2a annealed at 1700 °C, which clearly show the presence of HfC. Since, during the conversion of HfN into HfC, nitrogen is released, it is obvious that this reaction is

Table 6. Fraction of SiC_2N_2, SiC_4, and $SiCN_3$ and SiN_4 sites of SiHfBCN2b, as Derived from Gaussian Line Fitting of the ^{29}Si NMR Spectra from Figure 13

	SiC_4		SiC_2N_2		$SiCN_3$		SiN_4	
annealing temperature (°C)	δ (ppm)	site fraction (%)	δ (ppm)	site fraction (%)	δ (ppm)	site fraction (%)	δ (ppm)	site fraction (%)
1300	−19	20.1			−31	20.1	−49	59.7
1500	−18	55.3			−35	10.1	−50	34.6
1700	−19	67.5					−50	32.5

dx.doi.org/10.1021/ic501512p | Inorg. Chem. 2014, 53, 10443−10455

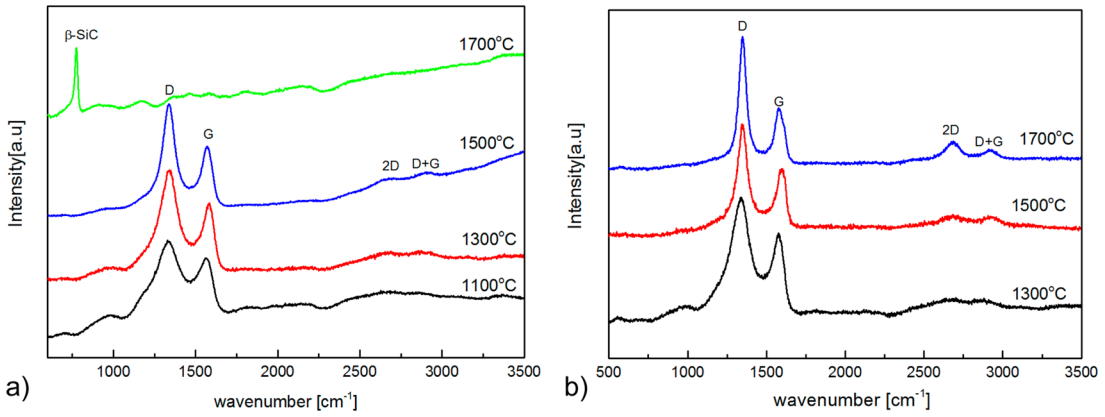

Figure 15. Raman spectra of the SiHfBCN-based samples annealed at different temperatures: (a) SiHfBCN2a (annealing in argon atmosphere) and (b) SiHfBCN2b (nitrogen atmosphere).

Table 7. Peak Positions, Integral Area Ratios (A_D/A_G and A_{2D}/A_D), Crystallite Lateral Size (L_a, L_{eq}), and Full Width at Half Maximum (fwhm) of the D and G Modes for the Segregated Carbon Phase Present in SiHfBCN Annealed in Ar and N_2 at Different Temperatures

sample	temperature (°C)	A_D/A_G	ω_D (cm^{-1})	$fwhm_D$ (cm^{-1})	ω_G (cm^{-1})	A_{2D}/A_D	L_{eq} (nm)	L_D(nm)
SiHfBCN2a-1100	1100	3.35	1335	155	1565	0.10	0.88	7.91
SiHfBCN2a-1300	1300	6.10	1342	113	1587	0.20	1.74	8.45
SiHfBCN2a-1500	1500	7.35	1337	89	1583	0.05	0.44	7.63
SiHfBCN2b-1300	1300	5.31	1338	136	1584	0.11	0.96	8.47
SiHfBCN2b-1500	1500	2.18	1347	80	1592	0.18	1.59	8.36
SiHfBCN2b-1700	1700	2.11	1348	55	1581	0.23	2.02	6.73

suppressed in a nitrogen atmosphere; thus, no HfC has been detected in the HT-annealed SiHfBCN2b samples.

The data from Figure 14 also explain the formation of HfB_2 upon annealing in an argon atmosphere and indicate that it can be generated from either HfN (or HfCN) and BCN (the BCN phase was stated to be present as phase-separated phase in the microstructure of SiBCN and has been approximated in the present assessment as a mixture of BN and B_4C). Thus, the formation of HfB_2 from HfN has been shown to be favorable within the entire investigated temperature range; whereas the conversion of HfCN into HfB_2 becomes favorable at temperatures beyond 1300 °C. Since, in both processes, gaseous N_2 is released as a side product, during the annealing experiments, the nitrogen partial pressure was unfavorable for the HfB_2 formation and, therefore, no HfB_2 was detected in the samples annealed in a N_2 atmosphere.

Considering the discussed data from the Ellingham diagram in Figure 14, there is clearly thermodynamic control of the high-temperature evolution of single-phase SiHfBCN, dictating the phase composition of the resulting UHTC-NCs upon HT annealing, which allows for the preparation of materials with tailored phase compositions.

The SiHfBCN ceramics annealed at temperatures from 1300 °C to 1700 °C in argon and nitrogen atmospheres were studied by means of Raman spectroscopy. The samples annealed in an argon atmosphere at 1300 and 1500 °C showed the presence of excess free carbon (see Figure 15a). Whereas the sample annealed in argon at 1700 °C did not contain free carbon; instead, the presence of β-SiC has been shown. The samples annealed in nitrogen atmosphere exhibited, independent of the annealing temperature, the presence of segregated carbon, as shown in Figure 15b. This is in agreement with the XRD, elemental analysis, and thermodynamic data, which show that annealing SiHfBCN in an argon atmosphere leads to the consumption of segregated carbon at temperatures of >1500 °C, cf. $Si_3N_4 + 3C = 3\beta\text{-}SiC + 2\ N_2$. This reaction is suppressed in a nitrogen atmosphere and, thus, the segregated carbon phase is still present in SiHfBCN2b annealed at 1700 °C.

The segregated carbon present in the HT annealed samples was found to be highly disordered (see Table 7). The Raman spectra exhibit the G and D modes at 1580 and 1350 cm^{-1}, respectively, which are typical for carbon materials. Furthermore, overtone bands at 2700 and 2950 cm^{-1} (2D and D + G modes, respectively) were found in some spectra. In all spectra, the integral area of the D-band (A_D) is significantly larger than that of the G-band (A_G), indicating the disordered feature of the segregated carbon.[44] Furthermore, the degree of disorder was rationalized also on the basis of the parameter L_D (interdefect distance), which has been defined, cf. $I_D/I_G = C(\lambda)/L_D^2$.[44] Thus, L_D becomes smaller as the annealing temperature increases (i.e., for SiHfBCN2b_1300, L_D = 8.47 nm; for SiHfBCN2b_1700, L_D = 6.73 nm), illustrating that the structural organization of the carbon phase increases. This conclusion is supported by the decrease in the full width at half maximum (fwhm) of the bands, as well as by the increase of the intensity of the G′-band (see Figure 15 and Table 7).[44] Moreover, the evolution of the parameter L_{eq} (the lateral cluster size, which, however, takes into account the tortuosity of the graphene sheets, cf.[44]

$$L_{eq}\ (\text{nm}) = 8.8\left(\frac{A_{2D}}{A_D}\right)$$

indicates the same trend as that previously described (see Table 7), i.e. an increase in the ordering of carbon as the annealing temperature increases.

Considering the obtained results, the SiHfBCN-based material prepared upon pyrolysis of the Hf- and B-modified

dx.doi.org/10.1021/ic501512p | Inorg. Chem. 2014, 53, 10443−10455

polysilazane is greatly versatile, with regard to its crystallization behavior and evolution of the phase composition at high temperatures. In both argon and nitrogen atmospheres, high-temperature annealing of SiHfBCN leads to ceramic nanocomposites with interesting phase compositions (i.e., SiC/HfC(N)/HfB_2 in argon and Si_3N_4/HfNC/SiBCN in nitrogen), which are expected to be promising candidates for applications at (ultra)high temperatures and under extreme environmental conditions.

IV. CONCLUSIONS

Within the present study, a single-source preparative access toward hafnium-containing UHTC-NCs has been discussed. The presence of Hf and B within the molecular structure of the single-source precursor leads to low-temperature phase separation processes within the resulting SiHfBCN, which are thermodynamically controlled. They facilitate the crystallization of the studied samples upon annealing at higher temperatures and thus allow for preparing UHTC-NCs with phase compositions suitable for applications at ultrahigh temperatures and under harsh conditions. The presented single-source-precursor synthesis method is believed to be applicable for other phase compositions consisting of a UHTC phase (e.g., Group IV transition-metal borides, carbides, nitrides) dispersed within a silica-former matrix (SiC, Si_3N_4, SiCN, SiBCN, etc.).

AUTHOR INFORMATION

Corresponding Author

*E-mail: ionescu@materials.tu-darmstadt.de.

Notes

The authors declare no competing financial interest.

ACKNOWLEDGMENTS

The authors thank Ms. S. Kaur and Ms. C. Fasel for performing elemental and thermogravimetric analyses, as well as Mr. W. Li for his support with the Rietveld refinement of the XRD patterns. J.Y. acknowledges financial support from China Scholarship Council (CSC) during his stay at TU Darmstadt. Furthermore, financial support from the European Research Agency (FP7 FUNEA—Functional Nitrides for Energy Applications) and the Deutsche Forschungsgemeinschaft (DFG, No. SFB595) is gratefully acknowledged.

REFERENCES

(1) Squire, T. H.; Marschall, J. *J. Eur. Ceram. Soc.* **2010**, *30*, 2239–2251.
(2) Van Wie, D. M.; Drewry, D. G.; King, D. E.; Hudson, C. M. *J. Mater. Sci.* **2004**, *39*, 5915–5924.
(3) Wuchina, E. J.; Opila, E.; Opeka, M. M.; Fahrenholtz, W.; Talmy, I. G. *Interface* **2007**, *16*, 30–36.
(4) Opeka, M. M.; Talmy, I. G.; Zaykoski, J. A. *J. Mater. Sci.* **2004**, *39*, 5887–5904.
(5) Blum, Y. D.; Kleebe, H. J. *J. Mater. Sci.* **2004**, *39*, 6023–6042.
(6) Fahrenholtz, W. G.; Hilmas, G. E.; Talmy, I. G.; Zaykoski, J. A. *J. Am. Ceram. Soc.* **2007**, *90*, 1347–1364.
(7) Paul, A.; Jayaseelan, D. D.; Venugopal, S.; Zapata-Solvas, E.; Binner, J.; Vaidhyanathan, B.; Heaton, A.; Brown, P.; Lee, W. E. *Am. Ceram. Soc. Bull.* **2012**, *91*, 22–28.
(8) Fahrenholtz, W. G.; Hilmas, G. E. *Int. Mater. Rev.* **2012**, *57*, 61–72.
(9) Ionescu, E.; Kleebe, H. J.; Riedel, R. *Chem. Soc. Rev.* **2012**, *41*, 5032–5052.
(10) Papendorf, B.; Nonnenmacher, K.; Ionescu, E.; Kleebe, H. J.; Riedel, R. *Small* **2011**, *7*, 970–978.
(11) Ionescu, E.; Linck, C.; Fasel, C.; Muller, M.; Kleebe, H. J.; Riedel, R. *J. Am. Ceram. Soc.* **2010**, *93*, 241–250.
(12) Ionescu, E.; Francis, A.; Riedel, R. *J. Mater. Sci.* **2009**, *44*, 2055–2062.
(13) Ionescu, E.; Papendorf, B.; Kleebe, H. J.; Riedel, R. *J. Am. Ceram. Soc.* **2010**, *93*, 1783–1789.
(14) Linck, C.; Ionescu, E.; Papendorf, B.; Galuskova, D.; Galusek, D.; Sajgalik, P.; Riedel, R. *Int. J. Mater. Res.* **2012**, *103*, 31–39.
(15) Papendorf, B.; Ionescu, E.; Kleebe, H. J.; Linck, C.; Guillon, O.; Nonnenmacher, K.; Riedel, R. *J. Am. Ceram. Soc.* **2013**, *96*, 272–280.
(16) Bernard, S.; Majoulet, O.; Sandra, F.; Malchere, A.; Miele, P. *Adv. Eng. Mater.* **2013**, *15*, 134–140.
(17) Mera, G.; Navrotsky, A.; Sen, S.; Kleebe, H. J.; Riedel, R. *J. Mater. Chem. A* **2013**, *1*, 3826–3836.
(18) Iwamoto, Y.; Kikuta, K.; Hirano, S. *J. Ceram. Soc. Jpn.* **2000**, *108*, 350–356.
(19) Wang, H.; Gao, B.; Chen, X. B.; Wang, J.; Chen, S. G.; Gou, Y. Z. *Appl. Organomet. Chem.* **2013**, *27*, 166–173.
(20) Wang, H.; Chen, X.; Gao, B.; Wang, J.; Wang, Y.; Chen, S.; Gou, Y. *Appl. Organomet. Chem.* **2013**, *27*, 79–84.
(21) Kimura, Y.; Kubo, Y.; Hayashi, N. *Compos. Sci. Technol.* **1994**, *51*, 173–179.
(22) Muller, A.; Gerstel, P.; Weinmann, M.; Bill, J.; Aldinger, F. *Chem. Mater.* **2002**, *14*, 3398–3405.
(23) Traßl, S.; Suttor, D.; Motz, G.; Rössler, E.; Ziegler, G. *J. Eur. Ceram. Soc.* **2000**, *20*, 215–225.
(24) Bill, J.; Seitz, J.; Thurn, G.; Durr, J.; Canel, J.; Janos, B. Z.; Jalowiecki, A.; Sauter, D.; Schempp, S.; Lamparter, H. P.; Mayer, J.; Aldinger, F. *Phys. Status Solidi A* **1998**, *166*, 269–296.
(25) Kroke, E.; Li, Y. L.; Konetschny, C.; Lecomte, E.; Fasel, C.; Riedel, R. *Mater. Sci. Eng., R* **2000**, *26*, 97–199.
(26) Li, Y. L.; Kroke, E.; Riedel, R.; Fasel, C.; Gervais, C.; Babonneau, F. *Appl. Organomet. Chem.* **2001**, *15*, 820–832.
(27) Ionescu, E.; Papendorf, B.; Kleebe, H. J.; Breitzke, H.; Nonnenmacher, K.; Buntkowsky, G.; Riedel, R. *J. Eur. Ceram. Soc.* **2012**, *32*, 1873–1881.
(28) Tsetsgee, O., *Solid State NMR Studies on Precursor-Derived Si-B-C-N and B-C-N Ceramics*. PhD Thesis, University of Stuttgart, 2009.
(29) MacKenzie, K. J.; Smith, M. E. *Multinuclear Solid-State Nuclear Magnetic Resonance of Inorganic Materials*; Elsevier: Amsterdam, 2002; Vol. *6*.
(30) Ziegler, G.; Kleebe, H. J.; Motz, G.; Muller, H.; Trassl, S.; Weibelzahl, W. *Mater. Chem. Phys.* **1999**, *61*, 55–63.
(31) Haluschka, C.; Kleebe, H. J.; Franke, R.; Riedel, R. *J. Eur. Ceram. Soc.* **2000**, *20*, 1355–1364.
(32) Kleebe, H. J.; Stormer, H.; Trassl, S.; Ziegler, G. *Appl. Organomet. Chem.* **2001**, *15*, 858–866.
(33) Trassl, S.; Kleebe, H. J.; Stormer, H.; Motz, G.; Rossler, E.; Ziegler, G. *J. Am. Ceram. Soc.* **2002**, *85*, 1268–1274.
(34) Gerardin, C.; Taulelle, F.; Bahloul, D. *J. Mater. Chem.* **1997**, *7*, 117–126.
(35) Sauter, D.; Weinmann, M.; Berger, F.; Lamparter, P.; Muller, K.; Aldinger, F. *Chem. Mater.* **2002**, *14*, 2859–2870.
(36) Widgeon, S.; Mera, G.; Gao, Y.; Sen, S.; Navrotsky, A.; Riedel, R. *J. Am. Ceram. Soc.* **2013**, *96*, 1651–1659.
(37) Trassl, S.; Motz, G.; Rössler, E.; Ziegler, G. *J. Non-Cryst. Solids* **2001**, *293*, 261–267.
(38) Trassl, S.; Motz, G.; Rössler, E.; Ziegler, G. *J. Am. Ceram. Soc.* **2002**, *85*, 239–244.
(39) Seifert, H. J.; Peng, J.; Lukas, H. L.; Aldinger, F. *J. Alloys Compd.* **2001**, *320*, 251–261.
(40) Lee, J. S.; Butt, D. P.; Baney, R. H.; Bowers, C. R.; Tulenko, J. S. *J. Non-Cryst. Solids* **2005**, *351*, 2995–3005.
(41) Weinmann, M.; Schuhmacher, J.; Kummer, H.; Prinz, S.; Peng, J. Q.; Seifert, H. J.; Christ, M.; Muller, K.; Bill, J.; Aldinger, F. *Chem. Mater.* **2000**, *12*, 623–632.
(42) Taylor, K. M. *Boron Nitride–Metal Carbide Bodies and the Manufacture Thereof*. U.S. Patent 2,888,355, May 26, 1959.
(43) Blum, Y.; Kleebe, H.-J. *J. Mater. Sci.* **2004**, *39*, 6023–6042.

(44) Ferreira, E. M.; Moutinho, M. V.; Stavale, F.; Lucchese, M.; Capaz, R. B.; Achete, C.; Jorio, A. *Phys. Rev. B* **2010**, *82*, 125429.
(45) Larouche, N.; Stansfield, B. L. *Carbon* **2010**, *48*, 620−629.